Hindawi Publishing Corporation
Advances in Condensed Matter Physics
Volume 2015, Article ID 531498, 10 pages
http://dx.doi.org/10.1155/2015/531498

Research Article

Two-Dimensional Metallicity with a Large Spin-Orbit Splitting: DFT Calculations of the Atomic, Electronic, and Spin Structures of the Au/Ge(111)-$(\sqrt{3} \times \sqrt{3})R30^\circ$ Surface

Andrzej Fleszar and Werner Hanke

Institut für Theoretische Physik und Astrophysik, Universität Würzburg, Am Hubland, 97074 Würzburg, Germany

Correspondence should be addressed to Andrzej Fleszar; fleszar@physik.uni-wuerzburg.de

Received 10 November 2014; Accepted 26 January 2015

Academic Editor: Victor V. Moshchalkov

Density functional theory (DFT) is applied to study the atomic, electronic, and spin structures of the Au monolayer at the Ge(111) surface. It is found that the theoretically determined most stable atomic geometry is described by the conjugated honeycomb-chained-trimer (CHCT) model, in a very good agreement with experimental data. The calculated electronic structure of the system, being in qualitatively good agreement with the photoemission measurements, shows fingerprints of the many-body effects (self-interaction corrections) beyond the LDA or GGA approximations. The most interesting property of this surface system is the large spin splitting of its metallic surface bands and the undulating spin texture along the hexagonal Fermi contours, which highly resembles the spin texture at the Dirac state of the topological insulator Bi_2Te_3. These properties make this system particularly interesting from both fundamental and technological points of view.

1. Introduction

Two-dimensional metallic systems are of particular theoretical and technological interests for the richness of physical phenomena they display and the possibility of their tuning in a controlled way. Recently, special attention has been paid to spin properties of such systems which are relevant to the potential applicability in the spintronics devices. In the surface systems the space inversion symmetry is broken. This fact together with the spin-orbit interaction leads to the momentum-spin locking, which protects against backscattering by potentials preserving the time-reversal symmetry. In this perspective, surfaces of the 3-dimensional topological insulators display the desired properties in their topological surface states [1, 2]. From the point of view of the integrability with the electronic technology, however, it would be specially desirable to find a semiconductor surface displaying both a good metallicity and a large spin splitting of its metallic surface bands. These properties have been recently found in the Ge(111) surface covered with a monolayer of a heavy metal. The β-phase of $(\sqrt{3} \times \sqrt{3})$-Pb/Ge(111) [3] and the $(\sqrt{3} \times \sqrt{3})$-Au/Ge(111) [4–6] systems possess metallic surface bands which are split by the strong spin-orbit interaction.

In this paper, we present results of detailed calculations based on the density functional theory (DFT) [7, 8] done for the $(\sqrt{3} \times \sqrt{3})R30^\circ$-Au/Ge(111) surface. We address the questions of the stability of the possible atomic configurations at this surface and the electronic and spin structures of the stable phase. We find that although the standard local-density approximation (LDA) and the gradient corrections to it (GGA) reproduce very well the experimental data on the geometry of this surface, that is, a ground-state property, the calculated electronic structure shows some characteristic deviations from the photoemission results, which point at the importance of the many-body effects for electronic excitations in this system, that is, quasiparticle excitations. We find that the self-interaction corrections (SIC) applied in a semiempirical way to the Au-5*d* states significantly improve the electronic structure: they partly correct the depth and the effective mass of the surface-state parabola and enhance

the amount of the hexagonal warping of the Fermi contour, bringing its shape closer to the experimental photoemission results. An important outcome of our calculations is the spin texture of the surface states split by the spin-orbit coupling (SOC). It turns out that, in addition to a very large value of the spin splittings of the surface bands, their spin texture shows the characteristic and searched features of the helical (keyword: Rashba [9]) and radial (keyword: Dresselhaus [10]) fingerprints, very similar to the recently theoretically predicted spin texture of the Dirac states of the topological insulator Bi_2Te_3 [11, 12].

In the next section, we present the methodology of calculations. In Section 3, the results of the theoretical determination of the surface geometry are discussed. Section 4 is devoted to the analysis of the electronic structure of the most stable geometry and the effect of the self-interaction corrections on the band structure. In Section 5, we discuss the spin texture at the Fermi contours.

2. Computational Details

The calculations in this work have been done within the density functional theory using the local-density approximation [7, 8] and the generalized gradient approximation (GGA) of the Perdew-Wang (PW91) type [13]. Two types of codes were applied. The plane-wave code of the QUANTUM ESPRESSO suite [14] has been used in studies of surface energies for various reconstructions models of the Au/Ge(111) system. For the detailed calculations of the electronic structure and spin texture of the most stable *conjugate-honeycomb trimer* (CHCT) model [15], our own mixed-basis codes were used, where, apart from plane waves in the basis, also *d*-type Gaussians were present in order to represent accurately the Au-5*d* orbitals. In both codes, the norm-conserving pseudopotentials have been employed. The surface was modelled using the periodic-slab construction, where a large number of germanium layers are terminated on one side with the Au adsorbates and on the opposite side the dangling bonds are saturated by the hydrogen atoms. Using asymmetric slabs is specially convenient when spin splittings are a goal of investigations. The whole slab is repeated periodically in the perpendicular-to-surface direction including a vacuum spacer between slabs. In the calculations of the atomic relaxations for different models of the surface the typical number of Ge-monolayers in the slab was 7. In the calculations of the electronic and spin structure for the most stable CHCT model, larger slabs, up to 25 Ge-monolayers, have been employed in order to disentangle the real surface features from the artificial quantization effects produced by the slab geometry. All calculations were done within the $(\sqrt{3} \times \sqrt{3})R30^{\circ}$ lateral unit cell with respect to the 1×1 unit cell of the unreconstructed Ge(111) surface. The lattice parameter of this hexagonal cell was fixed at the experimental value of 6.93 Å. In the self-consistency iterations, we have applied the (6,6,4) division of the Monkhorst and Pack method [16] and the "Gaussian smearing" technique of Fu and Ho [17] in determining the Fermi energy in metallic systems.

3. Results of Geometry Optimizations

Experimentally, two different studies done for the $(\sqrt{3} \times \sqrt{3})$-Au/Ge(111) system, the surface-X-ray-diffraction (XRD) of Howes et al. [18] and the low-energy electron-diffraction (LEED) of Over et al. [19], agree well with the CHCT model proposed for the Au deposition on the Si(111) surface [15] and also agree with each other in the values of determined atomic positions. A confirmation of the validity of the CHCT model brings also the recent STM study for this surface [20]. Correctness of the CHCT model might question, however, a certain disagreement between the electronic structure calculated on the basis of this model and results of the angular-resolved-photoemission (ARPES) measurements for this surface [4, 5, 20]. Although calculations done within LDA or GGA theory reproduce the metallic surface state seen in experiments, the theoretically determined bottom of this surface state is energetically too high, the electron-like Fermi surface contour is too spherical (shows less hexagonal warping compared with experiment), and the *k*-diameter of this contour is too small. The purpose of this section is to verify if the CHCT structural model describes indeed the most stable geometry of the Au/Ge(111) system and if some other model of this surface does not give a better agreement with the electronic structure determined by ARPES measurements.

In the search of an appropriate model, we limited ourselves to models of possibly high symmetry, compatible with the $\sqrt{3} \times \sqrt{3}$ periodicity and showing a trimerization of Au or Ge atoms seen in experiments. With these "boundary conditions" there is still place for variation of some parameters, such as the precise stoichiometry, the subsurface geometry (missing or not of the Ge-surface layer), or the point of placement of the trimers at the surface and their nature (Au or Ge trimers). We have considered altogether 22 geometrical models differing in the coverage of Au adatoms, in missing or not of the top Ge-surface layer (MTL or TL cases), in the placement of the characteristic structure (trimer) on top of T_1, T_4, or H_3 positions in the surface, and in the geometrical orientation of the apices of the trimer. The Au coverage was varied between the 1/3 one (1 Au atom in the $\sqrt{3} \times \sqrt{3}$ unit cell) and the 2/3, 3/3 (i.e., one Au monolayer), and 4/3 coverage. The atomic positions in each structural model were relaxed within the LDA approach and the surface energy was obtained according to the following formula:

$$E_{\text{surf}} = E_{\text{Total}} - \sum_i \mu_i N_i, \tag{1}$$

where E_{Total} is the total energy of the slab; μ_i and N_i are chemical potentials and number of atoms of the *i*th species in the slab. As the chemical potentials for Ge and Au, we have taken the energy per atom in the solid-state phase of these materials. It turned out that all structures with the Ge-TL configuration, as well as those with the 1/3 Au coverage, have much higher surface energies and could be therefore ruled out. Figure 1 shows top views of 9 most stable structures, all with the Ge-MTL configuration, together with the excess energy per surface unit cell of each structure over the most stable CHCT model.

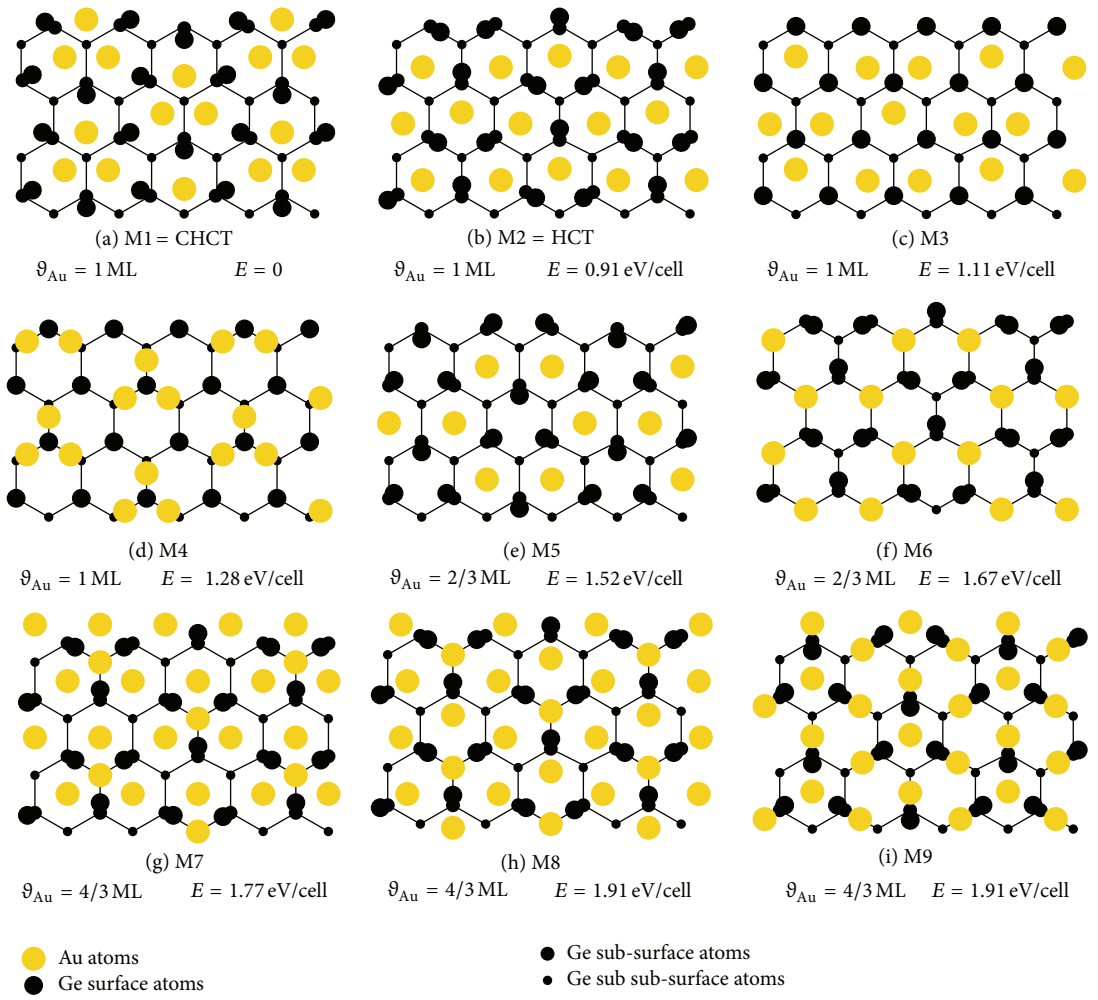

FIGURE 1: Top view of 9 energetically most favorable reconstruction models of the $(\sqrt{3} \times \sqrt{3})$-Au/Ge(111) surface. ϑ_{Au} is the Au coverage; E is the excess surface energy over the CHCT model.

Our LDA calculations clearly confirm the validity of the CHCT model for the $(\sqrt{3} \times \sqrt{3})$-Au/Ge(111) surface. The second realistic model, the honeycomb-chained-trimer model (HCT), which describes well the Ag adsorbates on the Si(111) surface [15], is still less favorable here. It is worth mentioning that in our calculations the HCT structure relaxes into the CHCT structure, when one allows for braking of the planar mirror symmetry by a slight rotation of the Ge-trimer at the beginning of the relaxation process.

In Table 1, we present calculated structural parameters for the CHCT model and compare them with the experimental values of [18, 19]. The parameters are defined in Figure 2. In the structural relaxation of the CHCT model, we have also used the GGA exchange-correlation functional in the PW91 form [13]. Both theories give very similar structural parameters and electronic band structures. The good agreement of theoretical and experimental parameters is another confirmation of the validity of the CHCT model.

TABLE 1: Atomic positions (in Å), as defined in Figure 2, obtained in this study within the LDA and GGA theories and reported in the surface-X-ray-diffraction (XRD, [18]) and low-energy electron-diffraction (LEED, [19]) experiments.

Parameter	LDA	GGA	XRD	LEED
	This study	This study	[18]	[19]
x_{Au}	1.62	1.65	1.63	1.62
x_{Ge_1}	4.07	4.09	4.11	4.07
x_{Ge_2}	4.54	4.54	4.59	4.58
z_{Au}	0.0	0.0	0.0	0.0
z_{Ge_1}	0.44	0.51	0.42	0.51
z_{Ge_2}	2.87	2.99	3.02	2.95
z_{Ge_3}	3.54	3.72	3.79	3.63
z_{Ge_4}	3.78	3.96	3.79	3.87
z_{Ge_5}	6.04	6.26	6.24	6.10
z_{Ge_6}	6.19	6.42	6.24	6.32
z_{Ge_7}	6.96	7.24	7.06	7.06

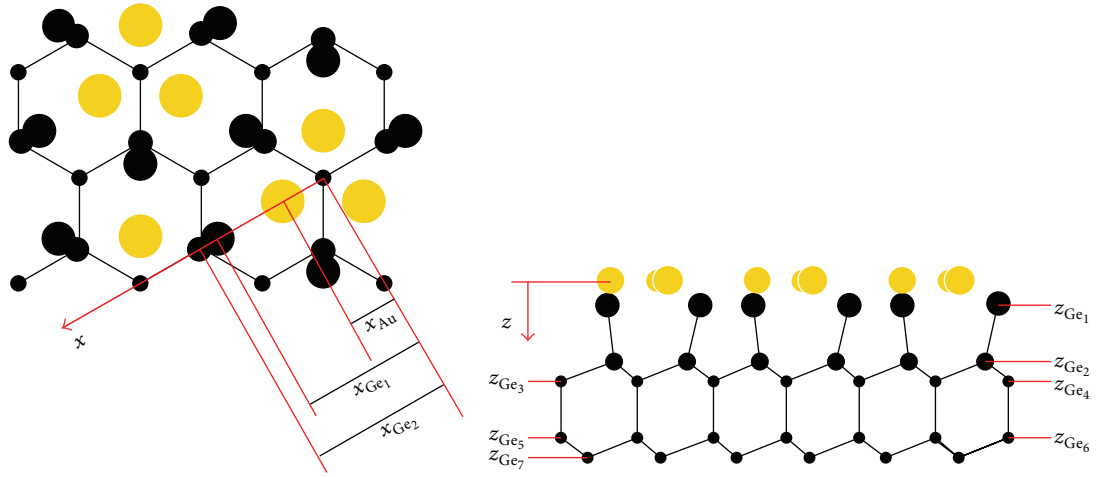

FIGURE 2: Top (a) and side (b) view of the CHCT model. The x parameters have origin at the T_4 position; the z parameters have their origin at the center of the Au overlayer.

4. Electronic Structure of the CHCT Model

For all geometrical models considered in the previous section, we have calculated also the electronic structure. It turned out that only the CHCT and the HCT models give rise to the electronic structures in a qualitative similarity with the ARPES results. All other models considered could be ruled out not only because of the unfavorable surface-formation energy, but also due to their electronic structure qualitatively different from experiment. The electronic structure of the HCT model being qualitatively correct, that is, displaying two metallic bands at the Fermi energy, inner hole-like and outer electron-like, is, however, worse in some detail than the CHCT model. In this section, we will analyze the electronic structure of the CHCT model, compare it with experiment, and discuss reasons of still remaining discrepancies with the experimental results. The main conclusion of this section is a suggestion that there is a significant component of the many-body physics not described correctly by the LDA or GGA theories, which is—at least partly—responsible for the discrepancies in experiment.

Figure 3(a) presents the LDA band structure of the CHCT model obtained with a slab consisting of 19 Ge layers, one Au layer at one surface, and hydrogen atoms saturating dangling bonds at the opposite surface. This slab contains altogether 63 atoms in one unit cell. The spin-orbit coupling is included. The band structure is shown along two high-symmetry directions of the surface Brillouin zone, the $\overline{M} - \overline{\Gamma}$ and the $\overline{\Gamma} - \overline{K}$. The energy zero is at the theoretical Fermi energy.

Concerning the metallic bands around the Fermi energy, one observes a number of hole-like bands with their maxima close to $\overline{\Gamma}$ and one (SOC split) electron-like, parabolic band. This is in a qualitative agreement with ARPES results presented in Figures 3, 4, and 5 of [4], though significant discrepancies are clearly seen. First of all, the electron-like parabola has its minimum at *ca.* 0.3 eV below the Fermi energy in the LDA calculation, whereas its experimental minimum is at *ca.* 1 eV below E_f. Second, the configuration of bands around E_f seems to be similar to experiment, however, only after shifting to higher energies of the theoretical Fermi energy. Without such a shift, the topmost hole-like metallic band is not well separated from the electron-like parabola at E_f and, moreover, the sizes (diameters) of the energy contours of LDA bands do not agree with experiment.

The necessity of shifting of E_f between calculations and experiment happens often for metallic surface systems. The most obvious reason for it is the charge flow between the semiconductor states (e.g., its impurity states) and the metallic band at the surface (Schottky effect). There are also unavoidable imperfections at the surface, like not precise stoichiometry, which result in a possible surplus charge and the formation of the band bendings close to surfaces. These effects are rather strong because, in the reduced dimensionality, that is, smaller density of states at a surface, an even small extra charge can lead to significant shifts of the Fermi energy. It is easy to see, however, that a simple shift of the Fermi level to higher energies cannot perfectly reconcile the experimental and theoretical results. In our opinion, the best overall agreement in the band structure close to the experimental Fermi energy is obtained with the 110 meV shift of the LDA Fermi level, shown in Figure 2(a) as a separate line. For such a shift, the hole-like bands seen in ARPES are reproduced pretty well, while the diameters of the constant-energy cut of the electron-like parabola are still too small. Obviously, the bottom of the electron-like parabola cannot be moved to its experimental position with such a small shift.

Searching for another possible reason of the discrepancy between theoretical and experimental band structures, we note that there are systematic errors of the LDA band structures of noble metals. These elements, similarly to elements of the IIB group of the periodic table, possess fully or almost fully occupied d electrons, which energetically are within the valence region of the elemental noble metals or

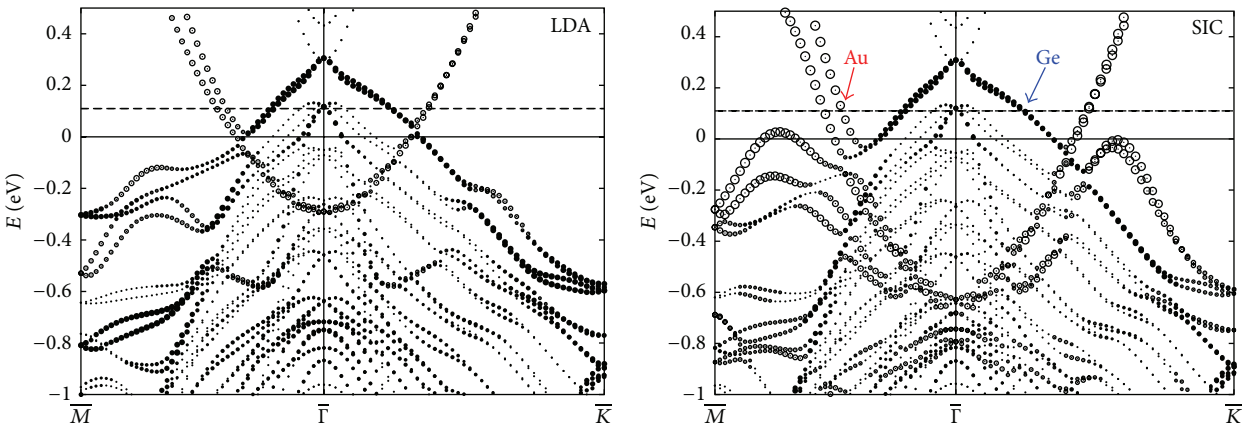

Figure 3: Electronic structure of the CHCT model obtained within the LDA theory (a) and with the SIC-corrected theory (b) along the $\overline{M}-\overline{\Gamma}-\overline{K}$ lines in the surface Brillouin zone. The red and blue arrows in the panel (b) show the states chosen for the presentation in Figure 4.

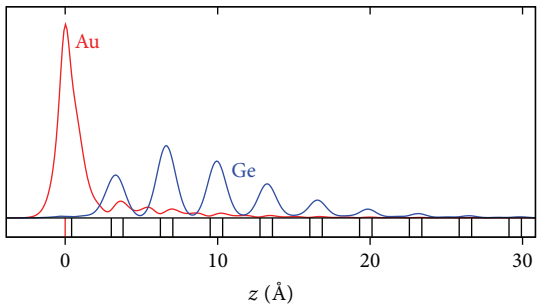

Figure 4: Planar average of the modulus square of the wave functions chosen in Figure 3(b). The red curve with the label "Au" corresponds to the surface state of the Au- and electron-like character. The blue curve with the label "Ge" corresponds to the Ge- and hole-like character. The z-zero is at the position of the Au-plane. The red and black balks in the bottom of the figure show the z positions of the Au and Ge atomic layers.

compounds with other elements. Within the LDA theory, these d electrons are energetically less bound (too high in energy) compared with experimental evidence. This LDA shift of the d bands can lead to an enhanced chemical hybridization of d and sp states in compounds containing these elements and thus can have an impact on the shape of bands in the vicinity of the Fermi energy. One of the reasons of this LDA shift—probably the biggest one—is the self-interaction error present in the LDA theory and particularly high for the localized d electrons. Therefore, elimination of this error could be helpful in bringing the theoretical band structure closer to experiment.

Because of the complexity of surface calculations, we have decided a simplified, semiempirical procedure of the self-interaction correction (SIC). In this procedure, we adjust the d component of the nonlocal Au atomic pseudopotential in such a way that the resulting bulk bands of the Au metal, in particular the 5d-Au bands, are in good agreement with photoemission measurements. In this way, we do not adjust the Au pseudopotential to the Au/Ge(111) system but rather search for a possibly universally correct Au-d pseudopotential. The same procedure applied in calculations of electron energy loss spectra in CdTe, where the Cd-4d states have been corrected, turned out to be essential in reproducing the experimental results [21].

Applying SIC to the $(\sqrt{3}\times\sqrt{3})$-Au/Ge(111) system results in a band structure in much better agreement with ARPES than was the case with the LDA method. However, some discrepancies still remain and it turns out that there is still need of shifting up the Fermi level. The best agreement is obtained again with the 110 meV shift. Figure 3(b) shows the resulting band structure when the SIC-corrected Au pseudopotential is used. The size of symbols along the band structure is proportional to the surface character of states. The empty (filled) symbols indicate states of predominantly gold (germanium) character. It can be seen that the electron-like parabola originates from the Au overlayer and the hole-like surface bands have a character of the Ge valence band shifted up due to the surface potential barrier. By comparing Figures 3(a) and 3(b), it is clear that the SIC had the biggest impact on the shape and position of the electron-like parabola. While the hole-like surface bands of germanium character are similar in both figures, the Au-derived electron parabola compares much better in Figure 3(b) with the experimental measurements of [4].

The red and blue arrows in Figure 3(b) show two chosen points at the electron-like surface band of Au character (red color) and at the hole-like surface band of Ge character (blue color), for which the shape of the wave function is shown in Figure 4. This figure presents the planar average of the modulus square of wave functions of both states as a function of the z-coordinate. The origin of z is at the position of the Au layer. The vacuum is at negative z; the Ge substrate is at positive z. The red short vertical line at $z = 0$ shows the position of Au atoms; the black short lines show positions of the next germanium layers. It follows from Figure 4 that both

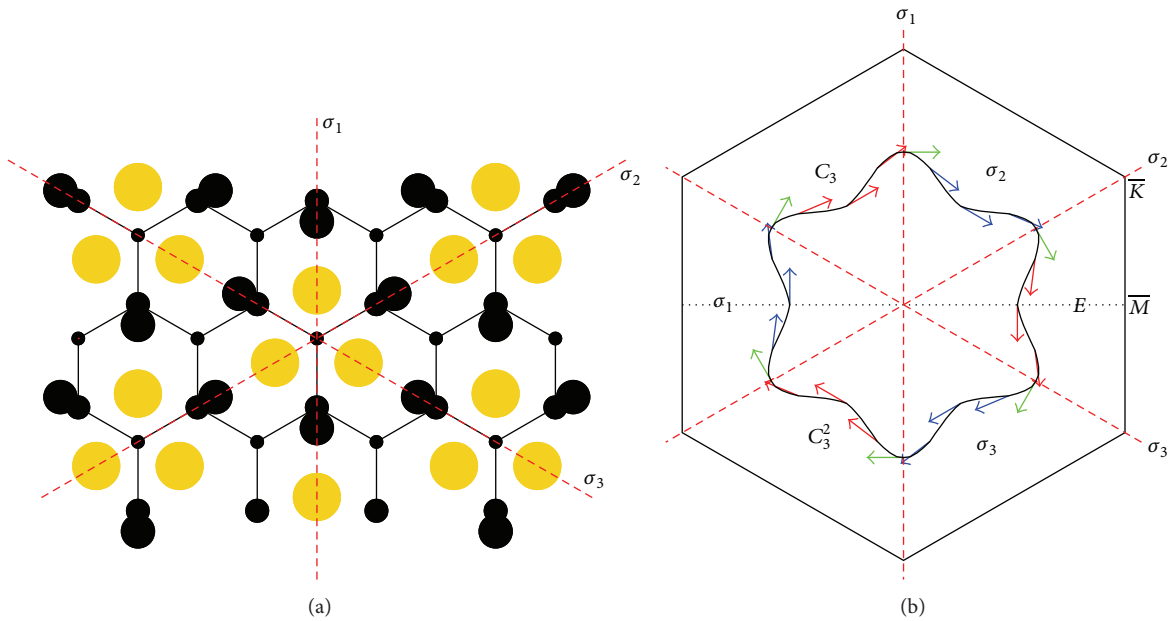

FIGURE 5: (a) Real-space top view of the CHCT structure with three mirror-plane symmetries σ_1, σ_2, and σ_3 shown as red, dashed lines. (b) The surface Brillouin zone of the $\sqrt{3} \times \sqrt{3}$ unit cell. The red, dashed lines show the orientation of the three mirror planes in the reciprocal space. The six symmetry operations of the C_{3v} group transform one of the irreducible parts of the BZ, called E, into other irreducible parts. A possible constant-energy contour is shown as a solid line within the BZ together with a possible spin texture along the contour shown as color arrows. Red color of arrows corresponds to one possible z direction of spin vectors; blue color corresponds to the opposite direction. The green color of spin vectors along the $\overline{\Gamma} - \overline{K}$ lines means fully planar spins.

surface bands have very different character. The electron-like surface band is very localized around the first two atomic layers. On the other hand, the hole-like surface band goes deep into the interior of the substrate. It has its maximum not directly at the surface but about 7 Å away from it and its shape resembles a bulk state modified by an envelope function produced by the quantum-well potential in the surface region.

5. Spin Texture of Surface Bands

Apart from the metallicity, one of the long searched properties of semiconductor-surface systems is the spin splitting of surface bands. The presence of a surface automatically leads to spin splittings of two-dimensional surface bands, known in the literature under the name of Rashba-Bychkov splitting [9]. Such a spin splitting is technologically interesting, because it can provide a way to produce spin-polarized currents via purely electronic means. The idealized Rashba spin pattern is planar; that is, the vectors of spin of particular states are oriented within the surface plane and are perpendicular to the 2-dimensional $\vec{k}$-vector of the state. Recently, additional perspectives have been found in the exploration of the three-dimensional orientation of the spin vector at the Fermi surface and its rotation towards the $\vec{k}$-radial or towards the out-of-surface-plane direction. The $(\sqrt{3} \times \sqrt{3})$-Au/Ge(111) system provides a particularly interesting example of such behavior. Due to the heavy-atom adsorption (Au) spin splittings are here amongst the largest ones so far reported experimentally for semiconductor surfaces decorated with adsorbates and exceed 210 meV at the Fermi energy. For similar systems, like Pb/Ge(111), a value of 200 meV for the spin splitting was reported [3]; for Tl coadsorbed at Au/Si(111) 190 meV has been measured [22]. In this section, we will analyze in detail the spin pattern of two pairs of surface bands, the electron-like Au-derived bands and the hole-like Ge-derived bands. Our analysis will be based on the generic features of symmetry and, therefore, will be applicable to all systems of the same symmetry, in particular, for example, to the Dirac edge states at the (111) surfaces of the topological insulators Bi_2Se_3 and Bi_2Te_3.

5.1. Symmetry Constraints in the Spin Texture. Figure 5 presents symmetry operations of the C_{3v} group both in real (a) and reciprocal (b) spaces in the $\sqrt{3} \times \sqrt{3}$ structure. The C_{3v} group has 6 symmetry operations: 3 rotations of the C_3 subgroup (E, C_3, and C_3^2) and 3 mirror planes (σ_1, σ_2, and σ_3), perpendicular to the surface plane, which in the reciprocal space intersect the 2-dimensional Brillouin zone (BZ) along the three $\overline{\Gamma} - \overline{K}$ directions. It is also shown in Figure 5(b) which particular symmetry transforms one irreducible part of the BZ (denoted as E) into all other irreducible parts. For illustration of general symmetry properties of the spin along a band, a typical constant-energy contour is shown in Figure 5(b). This contour could be one of the partners of the pair of surface bands of Au or Ge character, or, for example, a topological edge state in a 3-dimensional topological insulator such as Be_2Te_3. It is obvious that this constant-energy contour must show a bigger or smaller hexagonal

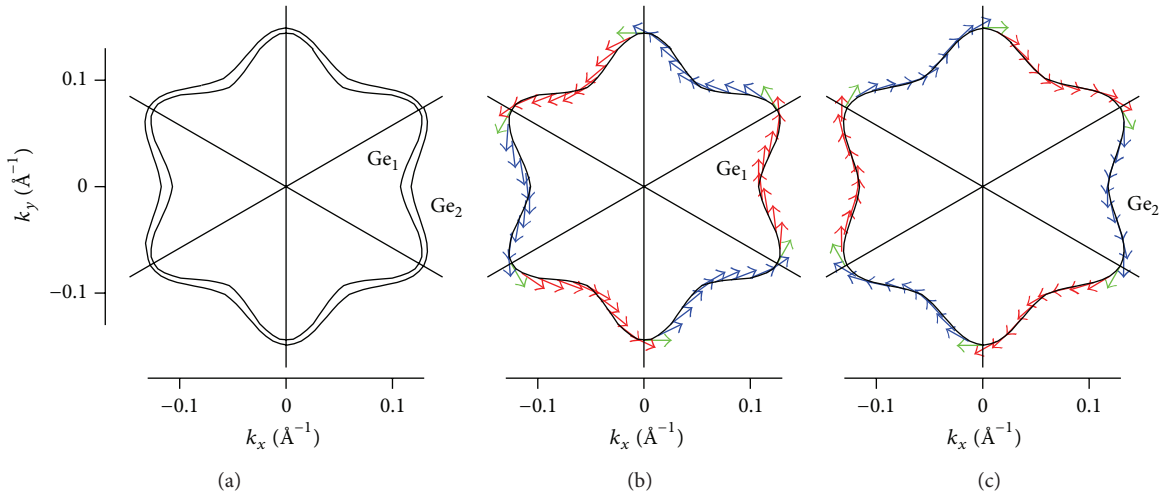

FIGURE 6: (a) Constant-energy contours at 110 meV above the theoretical Fermi energy for the hole-like bands of Ge character. The labels Ge_1 and Ge_2 correspond to the inner and outer contour, respectively. ((b) and (c)) Spin patterns along the inner and outer contours.

warping of its shape in agreement with the C_{3v} symmetry of the system. Figure 5(b) also shows a hypothetical spin texture along this hypothetical energy contour, which also must agree with the general symmetry-transformation properties of the spin. Since the spin vector can have all three (x, y, and z) directions and the presentation plane is the xy plane, we have shown with the blue color one possible z direction and with the red color the opposite one. Spin of a particular state, that is, the expectation value of the spin operator $\vec{S} = (\hbar/2)\vec{\sigma}$ (where $\vec{\sigma} = (\sigma_x, \sigma_y, \sigma_z)$ are Pauli matrices) at a particular (spinor) state, has symmetry-transformation properties of axial vectors. Under proper rotations, the spin vector "rotates" as normal vectors. Under space inversion, however, it remains unchanged. Since a mirror-plane symmetry is a combination of a proper rotation of 180 degrees with the inversion, it follows that, *for a nondegenerate state of $\vec{k}$-vector at the mirror plane, spin of this state must be perpendicular to the mirror plane*. It cannot have a nonzero component within the mirror plane. This means that for states along the $\overline{\Gamma} - \overline{K}$ directions spin vectors must be oriented in the surface plane and must be perpendicular to the $\overline{\Gamma} - \overline{K}$ directions. For nondegenerate states from the interior of the BZ, which are not at the $\overline{\Gamma} - \overline{K}$ lines, the spin values are not constrained by symmetry arguments and can have arbitrary directions. However, it follows from the same transformation rules of axial vectors that under the symmetry of a mirror plane their perpendicular components remain unchanged, whereas their planar (with respect to the symmetry plane) components are reversed. This means that going along the constant-energy contour of Figure 5(b) from the IBZ = E to the neighboring IBZ = σ_2 and IBZ = σ_3 the spin along the band must reverse its z-component. This behavior is illustrated in Figure 5(b), where the spin undulates along the Fermi contour: it reverses its z-component when rotating from one IBZ to the next. A special direction is also the $\overline{\Gamma} - \overline{M}$ direction, although it is not the mirror-plane symmetry direction. States along this line are invariant with respect to the combination of two symmetries: the time-reversal symmetry and the mirror-plane symmetry perpendicular to the $\overline{\Gamma} - \overline{M}$ line. This combination results in a particular constraint on the spin direction, which allows only for spins perpendicular to the $\vec{k}$-vector (unlike the $\overline{\Gamma} - \overline{K}$ direction, the z-component of spin is now allowed). The above considerations are valid *for nondegenerate states*. For degenerate states all spin directions are possible.

5.2. Spin Pattern along the Hole-Like and Electron-Like Fermi Contours. The symmetry-related constraints on the spin texture along a constant-energy contour are seen in both DFT calculations and the spin- and angular-resolved-photoemission measurements [6]. Figure 6 shows the calculated spin texture along the hole-like Fermi surface of Figure 3(b). In order to comply with the photoemission results, the constant-energy cut was taken at the 110 meV above the theoretical Fermi energy. In Figure 6(a), two spin-orbit split contours are shown; in Figures 6(b) and 6(c), the spin textures along the inner (Ge_1) and outer (Ge_2) contours are given, respectively. As in other cases this figure shows the surface from above; that is, the Ge crystal is below the picture plane. On each of the two contours spin vectors have a helical character, rotating anticlockwise at the inner contour and clockwise at the outer one. The blue/red color of spin vectors means the nonzero z-component directed inside/outside the crystal. The green color of arrow at the $\overline{\Gamma} - \overline{K}$ directions (mirror planes) means fully planar spins. Similarly, Figure 7 shows the spin texture at the constant-energy cut of the electron-like metallic band discussed in [6]. For this band better agreement with the photoemission results is obtained at the energy cut of 180 meV above the theoretical (SIC) Fermi level. It can be seen that the helicity of the Au-derived surface bands is opposite to the Ge-derived bands: spins at the inner band rotate clockwise and spins at the outer band rotate anticlockwise.

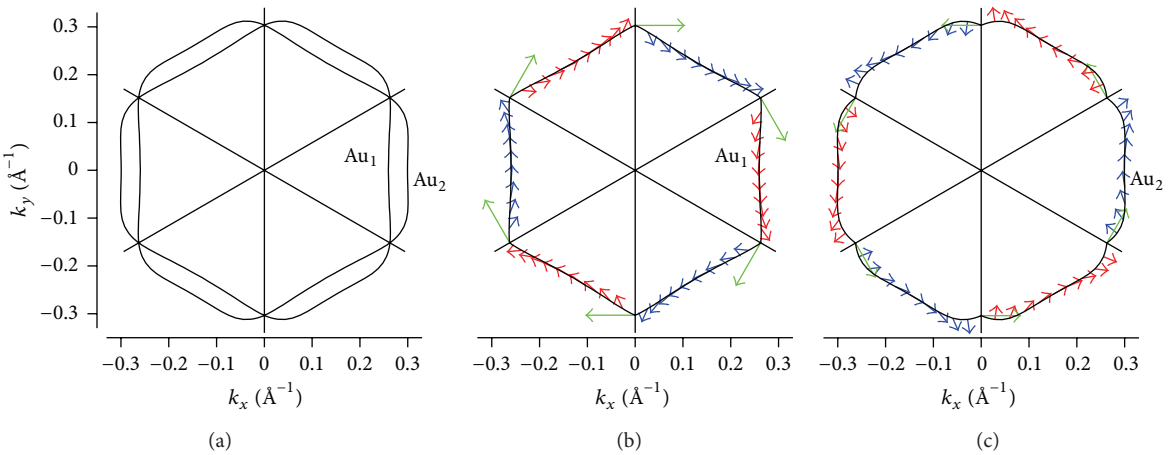

FIGURE 7: (a) Constant-energy contours at 180 meV above the theoretical Fermi energy for the electron-like bands of Au character. The labels Au_1 and Au_2 correspond to the inner and outer contour, respectively. The same as in Figure 6.

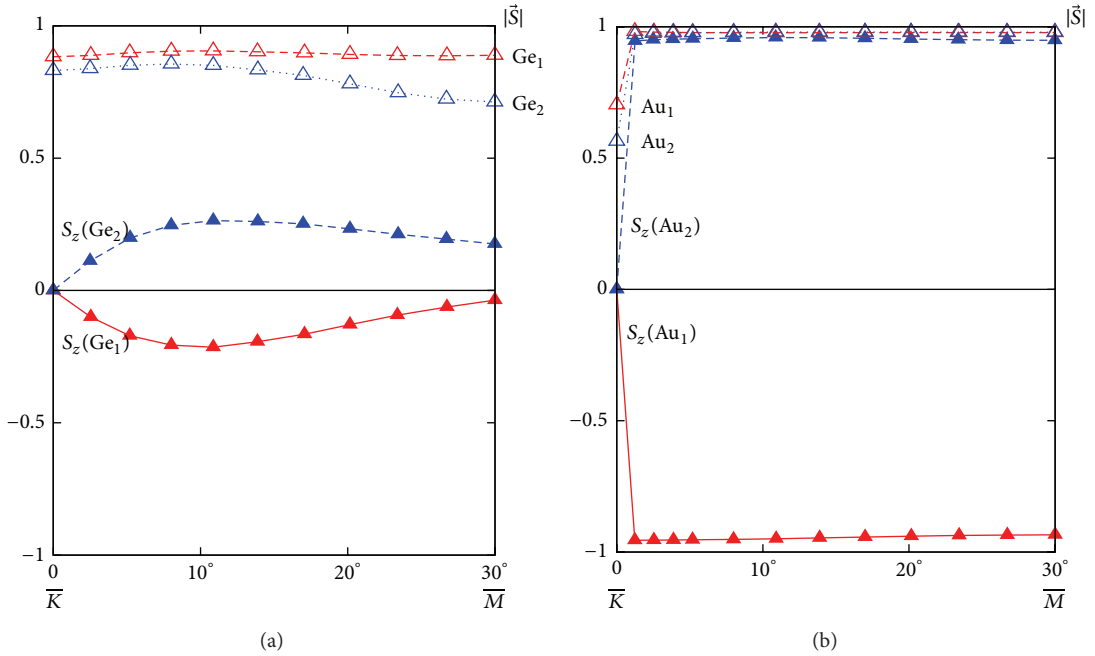

FIGURE 8: S_z components of spin vectors (filled triangles) along one arc of the bands between the $\overline{\Gamma} - \overline{K}$ and $\overline{\Gamma} - \overline{M}$ directions as a function of the scan angle, as well as the total spin polarization $|\vec{S}| = \sqrt{S_x^2 + S_y^2 + S_z^2}$ (empty triangles). The values of spins given in $\hbar/2$ units. (a) Ge-like contours of Figure 6 and (b) Au-like contours of Figure 7.

Figure 8 presents the values of the z-component along one portion of the hexagonally warped contour, as well as the total spin polarization, both in units of $\hbar/2$, for two pairs of bands. The total spin polarization is defined as the length of the measured spin vector: $|\vec{S}| = \sqrt{S_x^2 + S_y^2 + S_z^2}$. It is interesting to note that the total spin polarization is not equal to $\hbar/2$. This fact follows from the spin-orbit coupling in the presence of the spatial variation of the potential. When the variation of the potential in space is ignored, as is the case in models based on the $k \cdot p$ expansion (see next), the wave functions in the system are plane waves and the length of spin is automatically normalized. Please note that the spin polarization discussed in Figures 6 through 8 represents the spin properties of initial states of the photoemission process. The measured in spin-resolved ARPES experiments spin polarization of photo-electrons need not to be the same. As recently proposed by Park and Louie, the spin polarization of final states can differ from that of initial states due to the light polarization used in the excitation event [23]. Similarly, Herdt et al. suggested that the finite escape length of photoelectrons affects the measured spin polarization as well [24]. On the other hand, as reported in [6], for the $(\sqrt{3}\times\sqrt{3})$-Au/Ge(111) system, the theoretically predicted spin

polarization of initial photoemission states agrees very well with the spin polarization measured on photoelectrons.

Figures 6 through 8 show that the spin patterns of both pairs of bands differ in some detail. First difference is the opposite helicity direction for both pairs of bands. This, however, can be explained by the sign of the effective masses, that is, the hole-like or electron-like character of bands. Another difference is the dominant direction of the spin pattern: while the Ge-derived bands have an almost planar spin pattern, the Au-derived bands have spin vectors highly polarized along the surface normal (z direction). The z direction of spin vectors can be attributed to the fact that the Au adlayer is very close to the first Ge-surface layer. Such a geometry gives rise to potential gradients with a large planar component. Since the Au-derived bands are strongly localized at the first two surface layers, they accordingly strongly "feel" the planar gradients of the potential. In contrast, the Ge-derived surface bands are much extended inside the substrate (see Figure 4); therefore, they are not sensitive to the details of the potential within strict surface region. They are more sensitive to the long-range shape of the surface barrier due to the charge flow between crystal states and the metallic surface bands. Such a "macroscopic" shape of the surface barrier is, however, predominantly one-dimensional, along the z direction, which makes the spin texture of Ge-derived bands highly planar.

Yet another difference is in the special behavior of the direction of spin vectors for Au_1 and Au_2 bands close to $\overline{K}$ points. In the vicinity of these points, planar components of spin vectors start to be aligned with the $\vec{k}$ itself, that is, undergo rotations into the radial direction. Such a behavior is not within the idealized Rashba scenario, where the spin vectors are tangential to the energy contours and perpendicular to $\vec{k}$, and often appears in the literature as a fingerprint of the Dresselhaus spin-orbit splitting. The interplay of Rashba and Dresselhaus spin-orbit splittings has been considered as a prerequisite for certain types of spin manipulation, for example, in the nonballistic spin-field-effect transistor [25–28]. A comparison of Figures 6 and 7 shows that the Ge-derived surface states have more "Rashba-like" spin texture, whereas the Au-derived surface states have a more complex spin structure.

Interestingly, the spin texture of the Au_1 and Au_2 bands is similar to the one of the Dirac surface state of the topological insulator Bi_2Te_3. Fu [11] and Basak et al. [12] analyzed the spin texture of the Fermi-Dirac surface state in Bi_2Te_3 in terms of the $k \cdot p$ expansion. Fu pointed out the importance of a third-order term in the $k \cdot p$ expansion, which was responsible for two effects: the hexagonal warping of the constant-energy contours of the Dirac state and the generation of the perpendicular component of the spin vector. Basak et al. added to this expansion a fifth-order term which generates the radial rotations of the planar component of spin vectors in the vicinity of $\overline{K}$ points. In our recent publication, we have proposed another (a sixth-order) term, which is responsible for the hexagonal warping of the Fermi surface but does not affect the spin texture [6]. This proposition was justified by the fact that the hexagonal warping of bands in the $(\sqrt{3} \times \sqrt{3})$-Au/Ge(111) surface system is not an entire effect of the spin-orbit interaction but is a product—at least partially—of the crystal symmetry alone. Our $k \cdot p$ representation of the Au_1 and Au_2 bands in the vicinity of the Fermi energy has the following form:

$$H(k) = \left(\frac{\hbar^2 k^2}{2m^*} - C + c_h\left(k_+^6 + k_-^6\right)\right)\sigma_0 + v\left(k_x\sigma_y - k_y\sigma_x\right) + \lambda\left(k_+^3 + k_-^3\right)\sigma_z + i\zeta\left(k_+^5\sigma_+ - k_-^5\sigma_-\right). \quad (2)$$

In (2), σ_0 is the 2×2 identity matrix, σ_x, σ_y, and σ_z are Pauli matrices, $\sigma_\pm = \sigma_x \pm i\sigma_y$, and $k_\pm = k_x \pm ik_y$. For the following choice of parameters: $m^* = 0.4m_e$, $C = 0.77$ eV, $c_h = 70$ eV Å^6, $v = -0.1$ eV Å, $\lambda = -7$ eV Å^3, $\zeta = 5.5$ eV Å^5, and the $E = 0$ energy surface of this Hamiltonian model reproduces well both the Fermi contour and the spin structure of the metallic surface band in the $\sqrt{3} \times \sqrt{3}$-Au/Ge(111) surface (in the supplementary material in [6] an error appeared in the units of c_h, v, λ, and ζ parameters; the Å unit present in these parameters should be given in *positive* powers instead of *negative*, as was the case in [6]). We note that our $k \cdot p$ representation, (2), does not describe the Au_1 and Au_2 bands along their whole k-dispersion but is only valid in the vicinity of the Fermi energy shifted by the 180 meV above the theoretical, DFT Fermi level.

6. Conclusions

The $(\sqrt{3} \times \sqrt{3})$-Au/Ge(111) surface system has been theoretically investigated by means of the density functional theory. Comparing different reconstruction models compatible with the $\sqrt{3} \times \sqrt{3}$ geometry, we have shown that the CHCT model is energetically the most stable and in the same time gives rise to the surface electronic structure in best agreement with the results of photoemission measurements. It was shown that the self-interaction corrections strongly improve the LDA band structure. But there are still some deviations compared to experiment which point the importance of other many-body components in the electronic excitation spectrum of this system. Two types of metallic surface bands have been analyzed: the hole-like surface band of a predominantly Ge character and the electron-like surface band of a Au character. Both bands are split by the spin-orbit interaction into pairs of bands. The character of the spin texture close to the Fermi levels at each of these bands has been analyzed and related to the spatial properties of wave functions. In particular, the spin texture of the strongly spin-split metallic band of Au character has been modelled by means of the $k \cdot p$ expansion, following the ideas of [11, 12].

Conflict of Interests

The authors declare that there is no conflict of interests regarding the publication of this paper.

Acknowledgments

The authors acknowledge discussions with Jörg Schäfer, Philipp Höpfner, and Ralf Claessen. Calculations have been done at the Jülich Supercomputing Centre within Project hwb03. This work was supported by the DFG, FOR 1162, Grant.

References

[1] M. Z. Hasan and C. L. Kane, "Colloquium: topological insulators," *Reviews of Modern Physics*, vol. 82, no. 4, pp. 3045–3067, 2010.

[2] X.-L. Qi and S.-C. Zhang, "Topological insulators and superconductors," *Reviews of Modern Physics*, vol. 83, no. 4, pp. 1057–1110, 2011.

[3] K. Yaji, Y. Ohtsubo, S. Hatta et al., "Large Rashba spin splitting of a metallic surface-state band on a semiconductor surface," *Nature Communications*, vol. 1, no. 2, article 17, 2010.

[4] P. Höpfner, J. Schäfer, A. Fleszar et al., "Electronic band structure of the two-dimensional metallic electron system Au/Ge(111)," *Physical Review B—Condensed Matter and Materials Physics*, vol. 83, no. 23, Article ID 235435, 2011.

[5] K. Nakatsuji, R. Niikura, Y. Shibata et al., "Anisotropic splitting and spin polarization of metallic bands due to spin-orbit interaction at the Ge(111)($\sqrt{3} \times \sqrt{3}$)$R30^\circ$-Au surface," *Physical Review B: Condensed Matter and Materials Physics*, vol. 84, no. 3, Article ID 035436, 2011.

[6] P. Höpfner, J. Schäfer, A. Fleszar et al., "Three-dimensional spin rotations at the fermi surface of a strongly spin-orbit coupled surface system," *Physical Review Letters*, vol. 108, no. 18, Article ID 186801, 2012.

[7] P. Hohenberg and W. Kohn, "Inhomogeneous electron gas," *Physical Review*, vol. 136, article B864, 1964.

[8] W. Kohn and L. J. Sham, "Self-consistent equations including exchange and correlation effects," *Physical Review*, vol. 140, no. 4, pp. A1133–A1138, 1965.

[9] Y. Bychkov and E. I. Rashba, "Properties of a 2D electron gas with lifted spectral degeneracy," *JETP Letters*, vol. 39, no. 2, p. 78, 1984.

[10] G. Dresselhaus, "Spin-orbit coupling effects in zinc blende structures," *Physical Review*, vol. 100, no. 2, pp. 580–586, 1955.

[11] L. Fu, "Hexagonal warping effects in the surface states of the topological insulator Bi_2Te_3," *Physical Review Letters*, vol. 103, no. 26, Article ID 266801, 4 pages, 2009.

[12] S. Basak, H. Lin, L. A. Wray et al., "Spin texture on the warped Dirac-cone surface states in topological insulators," *Physical Review B*, vol. 84, Article ID 121401, 2011.

[13] J. P. Perdew and Y. Wang, "Accurate and simple analytic representation of the electron-gas correlation energy," *Physical Review B*, vol. 45, no. 23, pp. 13244–13249, 1992.

[14] P. Giannozzi, S. Baroni, N. Bonini et al., "QUANTUM ESPRESSO: a modular and open-source software project for quantum simulations of materials," *Journal of Physics: Condensed Matter*, vol. 21, no. 39, Article ID 395502, 2009.

[15] Y. G. Ding, C. T. Chan, and K. M. Ho, "Theoretical investigation of the structure ($\sqrt{3} \times \sqrt{3}$)R30$^\times$ – Au/Si(111) of the surface," *Surface Science*, vol. 275, no. 3, pp. L691–L696, 1992.

[16] H. J. Monkhorst and J. D. Pack, "Special points for Brillouin-zone integrations," *Physical Review B*, vol. 13, no. 12, pp. 5188–5192, 1976.

[17] C.-L. Fu and K.-M. Ho, "First-principles calculation of the equilibrium ground-state properties of transition metals: applications to Nb and Mo," *Physical Review B*, vol. 28, no. 10, pp. 5480–5486, 1983.

[18] P. B. Howes, C. Norris, M. S. Finney, E. Vlieg, and R. G. van Silfhout, "Structure of Ge(111)$\sqrt{3} \times \sqrt{3}$ $R30^\circ$-Au determined by surface x-ray diffraction," *Physical Review B*, vol. 48, no. 3, pp. 1632–1642, 1993.

[19] H. Over, C. Wang, and F. Jona, "Atomic bond configuration of Ge(111)-($\sqrt{3} \times \sqrt{3}$)$R30^\circ$-Au: a low-energy electron-diffraction study," *Physical Review B*, vol. 51, article 4231, 1995.

[20] K. Nakatsuji, Y. Motomura, Ry. Niikura, and F. Komori, "Selective doping in a surface band and atomic structures of the Ge(111) ($\sqrt{3} \times \sqrt{3}$)$R30^\circ$–Au surface," *Journal of Physics: Condensed Matter*, vol. 25, no. 4, Article ID 045007, 2013.

[21] A. Fleszar and W. Hanke, "Dynamical density response of II-VI semiconductors," *Physical Review B*, vol. 56, no. 19, pp. 12285–12289, 1997.

[22] L. V. Bondarenko, D. V. Gruznev, A. A. Yakovlev et al., "Large spin splitting of metallic surface-state bands at adsorbate-modified gold/silicon surfaces," *Scientific Reports*, vol. 3, article 1826, 2013.

[23] C.-H. Park and S. G. Louie, "Spin polarization of photoelectrons from topological insulators," *Physical Review Letters*, vol. 109, Article ID 097601, 2012.

[24] A. Herdt, L. Plucinski, G. Bihlmayer et al., "Spin-polarization limit in Bi2Te3 Dirac cone studied by angle- and spin-resolved photoemission experiments and ab initio calculations," *Physical Review B—Condensed Matter and Materials Physics*, vol. 87, no. 3, Article ID 035127, 2013.

[25] J. Schliemann, J. C. Egues, and D. Loss, "Nonballistic spin-field-effect transistor," *Physical Review Letters*, vol. 90, no. 14, Article ID 146801, 2003.

[26] J. Fabian, A. Matos-Abiague, C. Ertler, P. Stano, and I. Žutić, "Semiconductor spintronics," *Acta Physica Slovaca*, vol. 57, no. 4-5, pp. 565–907, 2007.

[27] E. I. Rashba and A. L. Efros, "Orbital mechanisms of electron-spin manipulation by an electric field," *Physical Review Letters*, vol. 91, Article ID 126405, 2003.

[28] B. A. Bernevig, J. Orenstein, and S.-C. Zhang, "Exact SU(2) symmetry and persistent spin Helix in a spin-orbit coupled system," *Physical Review Letters*, vol. 97, Article ID 236601, 2006.